JOURNAL OF GUIDANCE, CONTROL, AND DYNAMICS
Vol. 28, No. 4, July–August 2005

Optimizing Finite-Burn, Round-Trip Trajectories with I_{sp} Constraints and Mass Discontinuities

Christopher L. Ranieri* and Cesar A. Ocampo†
University of Texas at Austin, Austin, Texas 78712

Two indirect trajectory optimization formulations are used to solve a multipoint boundary-value problem to compute fuel-optimal, time-constrained, round-trip, long-duration finite-burn trajectories. The first formulation uses two control discontinuities corresponding to the arrival at the target and the following departure. A second formulation, using a state equality constraint across the stay time to constrain the spacecraft to match the position and velocity of the target, verifies the boundary-value problem posed by the first formulation. The minimum propellant missions constrain the stay time to be greater than or equal to a specified value and the total round trip time to be less than or equal to a specified value. Additionally, the conditions for optimal round-trip trajectories with mass discontinuities at the target and upper and lower bounds on the specific impulse I_{sp} for variable I_{sp} engines are formulated. The results are applied to nuclear electric, constant, or variable-specific-impulse, human-crewed missions. Earth–Mars and Earth–Jupiter round-trip trajectories are found efficiently. Missions that detail a controllability "ceiling" for variable-specific-impulse engines with I_{sp} bounds and mass discontinuities are presented. Off-boundary solutions for the time inequality constraints are also discussed.

Nomenclature

c	=	exhaust velocity
$\boldsymbol{c}$	=	constraint vector for boundary-value problem
G	=	Bolza function
$\boldsymbol{g}$	=	gravity acceleration vector
H	=	Hamiltonian
J	=	cost function
m	=	spacecraft mass
P	=	power
$\boldsymbol{r}$	=	spacecraft position vector
S	=	switching function
SE	=	state equality constraint vector
$\boldsymbol{s}$	=	slack variables used with time inequality constraints
T	=	thrust
t	=	time
t_{stay}	=	stay time at target
$\boldsymbol{u}$	=	thrust unit vector
$\boldsymbol{u}_c$	=	control vector
$\boldsymbol{v}$	=	spacecraft velocity vector
$\boldsymbol{z}$	=	parameter vector for boundary-value problem
α	=	in-plane thrust angle
β	=	out-of-plane thrust angle
Δm	=	mass discontinuity
$\boldsymbol{\theta}$	=	Lagrange multiplier vector adjoined with slack variables
$\boldsymbol{\lambda}$	=	costate Lagrange multiplier vector
λ_m	=	mass Lagrange multiplier
$\boldsymbol{\lambda}_r$	=	position costate Lagrange multiplier vector
λ_v	=	magnitude of velocity costate Lagrange multiplier vector
$\boldsymbol{\lambda}_v$	=	velocity costate Lagrange multiplier vector
$\dot{\lambda}_v$	=	time derivative of the magnitude of the velocity costate multiplier vector
μ_{CB}	=	central-body's gravitational constant
$\boldsymbol{\Psi}$	=	kinematic constraints vector
$\boldsymbol{\omega}$	=	Lagrange multiplier vector adjoined with kinematic constraints

Subscripts

max	=	maximum value: thrust or power
opt	=	optimal value
s/c	=	spacecraft
T	=	target body (Earth at t_0, t_f; Mars/Jupiter at t_1, t_2)
uc	=	unconstrained

Introduction

A SYSTEMATIC application of the indirect method is used to determine an optimal, minimum propellant, long-duration finite-burn, round-trip trajectory between any two orbits around a common central body. Long-duration finite burn means that the engines are "on" for a significant portion of the trajectory, regardless of the thrust acceleration. The round-trip trajectory includes a specified minimum stay time at the target where the spacecraft coasts along with the target. The total time of flight is constrained to be less than or equal to a specified maximum time of flight. These inequality constraints are more general than those used in previous papers where the stay time and total time of flight are either free variables or fixed, user-specified values as shown in the work by Casalino and Colasurdo[1] and Casalino et al.[2] These inequality constraints are shown to open up the solution space, allowing for optimal trajectories to be found off the boundaries of the fixed-value constraints. The target system in this formulation can be another spacecraft, a planet, a moon, or any other celestial body that is orbiting the same central body as the spacecraft that is performing the transfer. For the missions presented, the planets are treated as zero-sphere-of-influence point masses moving around the sun (the only gravitating body) with a realistic data (JPL DE405 ephemerides).‡ The sample missions focus on high-power, fast round-trip missions to Mars and Jupiter. Figure 1 shows a schematic of this mission plan.

The optimal control problem is solved as an indirect optimization problem to minimize propellant usage; the associated

Presented as ASS Paper 2004-0231 at the AIAA/AAS Spaceflight Mechanics Meeting, Maui, HI, 8–12 February 2004; received 16 March 2004; revision received 27 July 2004; accepted for publication 8 August 2004.

*National Defense Science and Engineering Graduate Research Fellow, Department of Aerospace Engineering and Engineering Mechanics, 1 University Station C0600; cxr288@mail.utexas.edu.

†Assistant Professor, Department of Aerospace Engineering and Engineering Mechanics, 1 University Station C0600; cesar.ocampo@mail.utexas.edu.

‡Data available online at http://ssd.jpl.nasa.gov/eph_info.html [cited 18 Sept. 2003].

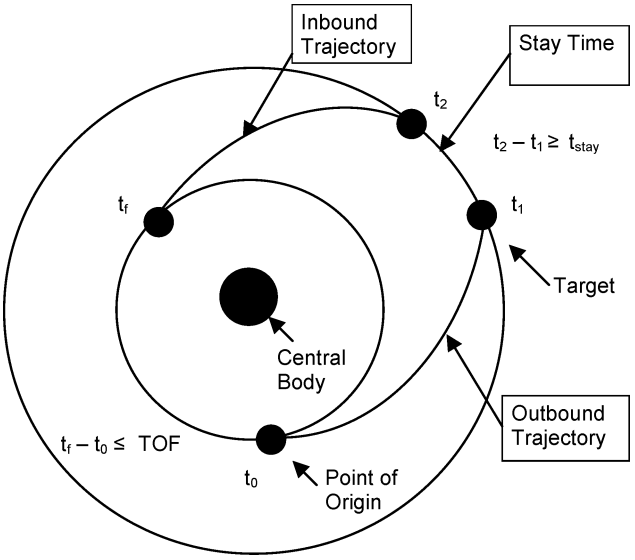

Fig. 1 Generalized round-trip, time-constrained trajectory.

Euler–Lagrange equations are integrated numerically, and the controls include the thrust direction and the constrained engine parameters. The start and end times of the inbound and outbound trajectories are constrained search variables. The resulting multipoint boundary-value problem is solved using the controls determined from the Pontryagin maximum principle.[3] A previous paper details the formulation of the optimal round-trip trajectory by deriving the first differential optimality conditions using this mission plan as a trajectory with two control corner conditions at which the Lagrange multipliers that control the trajectory might or might not be continuous.[4] This previous paper also provides an extensive review of other optimization methods applied to round-trip trajectory optimization and other uses of indirect methods for trajectory optimization.

Mass discontinuities at the target system at t_1 and t_2 are included in the optimal control formulation. For realistic mission scenarios, the spacecraft will most likely have a mass discontinuity at some point during the mission. These mass discontinuities can either increase or decrease the mass of the vehicle. A positive mass discontinuity corresponds to an increase in the spacecraft mass and can be used for sample return missions where the spacecraft's mass increases with the addition of a payload of scientific samples. A positive mass discontinuity can also account for picking up a propellant load to be used on the return trajectory; however, in the examples shown it will be assumed that all of the propellant needed for the mission is transported throughout. A negative mass discontinuity can represent a spent vehicle booster stage drop-off, mass left on the surface of a planet, supplies delivered to the target system, or fuel burned while in the target system.

Additionally, for variable-specific-impulse (VSI) engines, realistic upper and lower bounds are added for the specific impulse I_{sp} or thrust values, and the optimal control problem is adjusted to account for these additional constraints. An example of this type of engine is the VASIMR (Variable Specific Impulse Magnetoplasma Rocket) engine currently under development.[5] In contrast to a constant specific impulse engine (CSI), the variability of the I_{sp} or thrust of a VSI engine increases the performance of these missions, providing higher payload mass fractions. However, realistic trajectories for missions using engines such as VASIMR must include the engine specific upper and lower bounds for the I_{sp} or thrust, which limits the performance and extra degree of freedom of the VSI engine. The effects on the propellant usage from the bounds of VSI missions are illustrated in a comparison to unbounded VSI missions. The bounded VSI missions are still more efficient than comparable CSI missions.

The optimal control problem is reformulated in order to verify the boundary-value problem posed by the round-trip trajectory conditions found from using the two corner control discontinuities as shown by Ranieri and Ocampo.[4] Instead of using two control discontinuities to deal with the arrival and departure of the spacecraft at the target system, a state equality constraint is used. The state equality constraint enforces that the spacecraft always maintains zero relative position and velocity with its target during the entire stay time. The first formulation using the two corner control discontinuities requires that the position and velocity of the spacecraft match the target's position and velocity only at t_1 and t_2 but does not directly enforce this constraint across the stay time. Therefore, a feasible solution that satisfied all of the kinematic boundary constraints, but not necessarily all of the transversality conditions, could have the spacecraft match the target position and velocity at times t_1 and t_2. However, the spacecraft could thrust away from the target and then back to the target during the stay time between t_1 and t_2. This is obviously not an optimal stay time trajectory. Formulating the problem using the state equality constraint during the stay time removes this feasible solution and eliminates the user-specified zero-thrust value used during the stay time in the original formulation. The boundary-value problem posed by this method is shown to be identical to the original problem formulation.

System Equations and the Optimal Control Problem

First, the equations of motion of the trajectory are defined:

$$\dot{\boldsymbol{x}} = \begin{bmatrix} \boldsymbol{v} \\ \boldsymbol{g} + (T/m)\boldsymbol{u} \\ -T/c \end{bmatrix} \tag{1}$$

where

$$\boldsymbol{x} = \begin{bmatrix} \boldsymbol{r} \\ \boldsymbol{v} \\ m \end{bmatrix} \tag{2}$$

The force field is a time-invariant central body field:

$$\boldsymbol{g} = -\mu_{CB}\boldsymbol{r}/r^3 \tag{3}$$

For a CSI engine, the controls are defined as the thrust direction and the thrust magnitude:

$$\boldsymbol{u}_c = \begin{bmatrix} \boldsymbol{u} \\ T \end{bmatrix} \tag{4}$$

with constraints

$$|\boldsymbol{u}| = 1 \tag{5}$$

$$0 \leq T \leq T_{\max} \tag{6}$$

For a VSI engine, the controls are defined as the thrust direction, the exhaust velocity or thrust magnitude, and the power:

$$\boldsymbol{u}_c = \begin{bmatrix} \boldsymbol{u} \\ c \\ P \end{bmatrix} \quad \text{or} \quad \boldsymbol{u}_c = \begin{bmatrix} \boldsymbol{u} \\ T \\ P \end{bmatrix} \tag{7}$$

with constraints

$$|\boldsymbol{u}| = 1 \tag{8}$$

$$0 \leq P \leq P_{\max} \tag{9}$$

$$c = 2P/T \tag{10}$$

The cost function for the round-trip trajectory can be chosen to either maximize the final mass at the return to the point of origin for a user-specified initial mass or minimize the initial mass for a user-specified final mass. The Hamiltonian and Bolza functions are first presented using the two corner control discontinuities,[4] and the

modifications caused by the state equality constraint are introduced later:

$$H = \boldsymbol{\lambda}^T \dot{\boldsymbol{x}} = \boldsymbol{\lambda}_r^T \boldsymbol{v} + \boldsymbol{\lambda}_v^T \boldsymbol{g} + (T/m)\boldsymbol{\lambda}_v^T \boldsymbol{u} - (T/c)\lambda_m \tag{11}$$

$$-\dot{\boldsymbol{\lambda}}^T = \boldsymbol{H}_x \tag{12}$$

Equation (12) yields

$$\dot{\boldsymbol{\lambda}}_r = -\boldsymbol{\lambda}_v^T \left(\frac{\partial \boldsymbol{g}}{\partial \boldsymbol{r}}\right) \tag{13}$$

$$\dot{\boldsymbol{\lambda}}_v = -\boldsymbol{\lambda}_r \tag{14}$$

$$\dot{\lambda}_m = \left(\frac{T}{m^2}\right)\boldsymbol{\lambda}_v^T \boldsymbol{u} \tag{15}$$

The spacecraft must match the position and velocity of the target at t_1 and t_2 and also match the point of origin's position and velocity at t_0 and t_f. This yields four sets of physical state constraints that must be met for a valid solution when solving the problem using the two corner control discontinuities:

$$\boldsymbol{\psi}_i = \begin{bmatrix} \boldsymbol{r}_{s/c}(t_i) - \boldsymbol{r}_{Ti}(t_i) \\ \boldsymbol{v}_{s/c}(t_i) - \boldsymbol{v}_{Ti}(t_i) \end{bmatrix} = 0, \qquad i = 0, 1, 2, f \tag{16}$$

The inequality constraints on the stay time at the target and on the total time of flight are treated via slack variables. They allow the program to search for the optimal stay time greater than a minimum prescribed stay time and a time of flight (TOF) no longer than a prescribed total time of flight. Therefore, the times and corresponding states in this problem are search parameters:

$$t_2 = t_1 + t_{\text{stay}} + s_1^2 \tag{17}$$

$$t_f = t_0 + \text{TOF} - s_2^2 \tag{18}$$

These inequality constraints are then adjoined to the Bolza function with their own Lagrange multipliers. The Bolza function takes the form

$$G = m_f + \boldsymbol{\omega}_0^T \boldsymbol{\psi}_0 + \boldsymbol{\omega}_1^T \boldsymbol{\psi}_1 + \boldsymbol{\omega}_2^T \boldsymbol{\psi}_2 + \boldsymbol{\omega}_f^T \boldsymbol{\psi}_f + \theta_1\left(t_2 - t_1 - t_{\text{stay}} - s_1^2\right) + \theta_2\left(t_f - t_0 - \text{TOF} + s_2^2\right) \tag{19}$$

The spacecraft thrust direction is aligned with the primer vector as defined by Lawden[6]:

$$\boldsymbol{u} = \boldsymbol{\lambda}_v / \lambda_v \tag{20}$$

The time derivative of the mass multiplier, Eq. (15), can be rewritten using the thrust unit direction vector:

$$\dot{\lambda}_m = (T/m^2)\boldsymbol{\lambda}_v^T \boldsymbol{u} = \lambda_v T \Big/ m^2 \tag{21}$$

For the CSI engine, the well-known thrust switching function is defined as

$$S = \lambda_v / m - \lambda_m / c \tag{22}$$

For VSI engines, the thrust switching function is defined as

$$S_{\text{VSI,T}} = (\lambda_v / m) - T(\lambda_m)/(2P) \tag{23}$$

The partial of the Hamiltonian is taken with respect to the thrust to determine the optimal thrust value:

$$T_{\text{uc,opt}} = P_{\max}\lambda_v / (m\lambda_m) \tag{24}$$

If exhaust velocity is used as the control, a VSI power switching function is defined as

$$S_{\text{VSI,P}} = 2(\lambda_v / m - \lambda_m / c)/c \tag{25}$$

Following the same procedure as used to determine the optimal thrust value, the optimal exhaust velocity is shown to be

$$c_{\text{uc,opt}} = 2m\lambda_m / \lambda_v \tag{26}$$

Table 1 Thrust and exhaust velocity optimal values

Control variable	Control variable region	Optimal control value
T	$T_{\min} < T_{\text{uc, opt}} < T_{\max}$	$T_{\text{uc, opt}} = P\lambda_v/(m\lambda_m)$
T	$T_{\text{uc, opt}} \geq T_{\max}$	$T = T_{\max}$
T	$T_{\text{uc, opt}} \leq T_{\min}$; $S_{\text{VSI,T}} > 0$	$T = T_{\min}$
T	$T_{\text{uc, opt}} \leq T_{\min}$, $S_{\text{VSI,T}} < 0$	$T = 0$
c	$c_{\min} < c_{\text{uc, opt}} < c_{\max}$	$c_{\text{uc, opt}} = 2m\lambda_m/\lambda_v$
c	$c_{\text{uc, opt}} \leq c_{\min}$	$c = c_{\min}$
c	$c_{\text{uc, opt}} \geq c_{\max}$; $S_{\text{VSI,c}} > 0$	$c = c_{\max}$
c	$c_{\text{uc, opt}} \geq c_{\max}$; $S_{\text{VSI,c}} < 0$	$P = P_{\min} \quad \therefore T = 0$

I_{sp} or Thrust Bounds

In modeling these trajectories, it is more realistic to include upper and lower bounds to the control variable of either thrust or exhaust velocity (i.e., I_{sp}). Ocampo[7] and Casalino and Colasurdo[1] have discussed the derivation of these bounds previously. The applicable control laws are summarized in Table 1.

Optimality Conditions at Control Corner Discontinuities

The first differential of the cost function yields the following conditions for optimality under the control of the primer vector and with the costates governed by the costate equation (12). The derivation of these conditions closely follows the corner conditions laid out by Hull[8] and Bryson and Ho.[9] The conditions with plus or minus subscripts correspond to the value of the variable before (e.g., H_{1-}) or after (e.g., H_{1+}) the control corner at that time (e.g., t_1). The augmented cost function is

$$J = G + \int_{t0}^{tf} (H - \boldsymbol{\lambda}^T \dot{\boldsymbol{x}})\, \mathrm{d}t \tag{27}$$

The conditions at the initial state and time t_0 are

$$G_{t0} = H_0 \tag{28}$$

$$G_{x0} = -\boldsymbol{\lambda}_0^T \tag{29}$$

The conditions at the first corner at t_1 are

$$G_{s1} = 0 = -2\theta_1 s_1 \tag{30}$$

$$G_{\theta 1} = 0 = t_2 - t_1 - t_{\text{stay}} - s_1^2 \tag{31}$$

$$G_{t1} = H_{1+} - H_{1-} \tag{32}$$

$$G_{x1} = \boldsymbol{\lambda}_{1-}^T - \boldsymbol{\lambda}_{1+}^T \tag{33}$$

The conditions at the second corner at t_2 are

$$G_{s2} = 0 = 2\theta_2 s_2 \tag{34}$$

$$G_{\theta 2} = 0 = t_f - t_0 - \text{TOF} + s_2^2 \tag{35}$$

$$G_{t2} = H_{2+} - H_{2-} \tag{36}$$

$$G_{x2} = \boldsymbol{\lambda}_{2-}^T - \boldsymbol{\lambda}_{2+}^T \tag{37}$$

The conditions at the final state and time t_f are

$$G_{\text{tf}} = -H_f \tag{38}$$

$$G_{\text{xf}} = \boldsymbol{\lambda}_f^T \tag{39}$$

Using the simplifications spelled out in Ref. 4, the boundary-value problem can be formulated and posed. Adding the bounds on the I_{sp} or thrust values for the VSI engines does not directly affect the boundary-value problem.

Mass Discontinuities at the Target System

It is sometimes desirable to have a mass discontinuity Δm upon arrival at t_1 or at departure at t_2 from the target system. To add this functionality to the boundary-value problem, the Bolza function, Eq. (19), must be modified to reflect these changes in the spacecraft's state at times t_1 and t_2.

First, the mass discontinuity is defined and adjoined to the Bolza function:

$$\psi_m = \begin{bmatrix} m_{1+} & -m_{1-} & -\Delta m_1 \\ m_{2+} & -m_{2-} & -\Delta m_2 \end{bmatrix} = 0 \tag{40}$$

$$G = m_f + \boldsymbol{\omega}_0^T \psi_0 + \boldsymbol{\omega}_1^T \psi_1 + \boldsymbol{\omega}_2^T \psi_2 + \boldsymbol{\omega}_f^T \psi_f + \boldsymbol{\omega}_m^T \psi_m + \theta_1\left(t_2 - t_1 - t_{\text{stay}} - s_1^2\right) + \theta_2\left(t_f - t_0 - \text{TOF} + s_2^2\right) \tag{41}$$

With these modifications, taking the first differential of Eq. (27) yields most of the same conditions, Eqs. (28–39), found for the case without the mass discontinuity. However, Eqs. (33) and (37) no longer apply for the entire state vector. These equations, which describe the behavior of the Lagrange multipliers across the corners at t_1 and t_2, are still valid for the position and velocity components of the state vector but no longer for the spacecraft mass. A new set of equations must be used to describe the mass Lagrange multipliers at the corners t_1 and t_2.

The mass multiplier before and after the corner at t_1 is now described by

$$G_{m1-} = \lambda_{m1-} \tag{42}$$

$$G_{m1+} = -\lambda_{m1+} \tag{43}$$

Applying these equations to the new Bolza function, Eq. (41), yields that the mass discontinuity is again continuous across the corners, which is identical to the solution found for the case with no mass discontinuities[4]:

$$\lambda_{m1-} = \lambda_{m1+} \tag{44}$$

Combining Eqs. (32), (33) (for position and velocity multipliers only), and (44) yields the same results as found before for the behavior of the switching function at the corner.

$$S_{1-}T_{1-} - \theta_1 = 0 \tag{45}$$

The solution process is identical across the second corner at time t_2, and Eqs. (36) and (37) (for position and velocity multipliers only) reduce to a similar result:

$$\lambda_{m2-} = \lambda_{m2+} \tag{46}$$

$$S_{2+}T_{2+} - \theta_1 = 0 \tag{47}$$

This indicates that the product of the switching function and the thrust must be equal at the end of the outbound trajectory and at the start of the inbound trajectory. The same equality holds for the problem with no mass discontinuity[4]:

$$S_{2+}T_{2+} = S_{1-}T_{1-} \tag{48}$$

It is also found, as shown in Ref. 4,

$$S_0 T_0 = S_f T_f \tag{49}$$

The particular significance of Eq. (48) for a CSI engine, which has a constant thrust and exhaust velocity, is that the velocity multiplier magnitude is no longer the same at the end of the outbound and at the start of the inbound trajectories. This conclusion cannot necessarily be made for a VSI engine as the values for the thrust and exhaust velocity are not necessarily equal at times t_1 and t_2. As shown with Eqs. (45) and (47), the boundary-value problem is the same for trajectories with or without specified mass discontinuities at times t_1 and/or t_2 (Ref. 4).

Verification of Boundary-Value Problem

As mentioned earlier, the optimal control problem detailed in Ref. 4 is reformulated to verify the earlier theoretical results and to more rigorously deal with the stay time trajectory. The new optimal control formulation using the state equality constraint is solved by first adjoining the state equality constraint to the Hamiltonian. However, the state equality constraint is not directly added to the Hamiltonian. Rather, time derivatives of the state equality constraints on position and velocity are taken until each equality constraint has an explicit dependence on the control variables. The position equality constraints are defined as

$$\mathbf{SE}_r = (\boldsymbol{r}_{\text{s/c}} - \boldsymbol{r}_T)_{3\times 1} = 0 \tag{50}$$

Taking two time derivatives of the position equality constraint yields a constraint that is explicitly a function of the control variables T and $\boldsymbol{u}$:

$$\mathbf{SE}_r'' = \boldsymbol{a}_{\text{s/c}} - \boldsymbol{a}_T = [(T/m)\boldsymbol{u} + \boldsymbol{g} - \boldsymbol{a}_T]_{3\times 1} = 0 \tag{51}$$

The velocity equality constraints are defined as

$$\mathbf{SE}_v = (\boldsymbol{v}_{\text{s/c}} - \boldsymbol{v}_T)_{3\times 1} = 0 \tag{52}$$

Taking one time derivative of the velocity equality constraint yields a constraint that is also explicitly a function of the control variables T and $\boldsymbol{u}$:

$$\mathbf{SE}_v' = \boldsymbol{a}_{\text{s/c}} - \boldsymbol{a}_T = [(T/m)\boldsymbol{u} + \boldsymbol{g} - \boldsymbol{a}_T]_{3\times 1} = 0 \tag{53}$$

Because Eqs. (51) and (53) are identical, the state equality constraint is now represented as a the same control equality constraint that is then adjoined with a new Lagrange multiplier to the Hamiltonian as defined by Eq. (11). The new multiplier has a value of zero on the outbound and inbound trajectory legs, whereas it takes on a nonzero value during the stay time trajectory:

$$\mathbf{SE}_{\text{ST}} = (\mathbf{SE}_{\text{Stay Time}})_{3\times 1} = \mathbf{SE}_r'' = \mathbf{SE}_v' \tag{54}$$

The new Hamiltonian is defined as

$$\hat{H} = \boldsymbol{\lambda}_r^T \boldsymbol{v} + \boldsymbol{\lambda}_v^T \boldsymbol{g} + (T/m)\boldsymbol{\lambda}_v^T \boldsymbol{u} - (T/c)\lambda_m + \boldsymbol{\xi}^T \mathbf{SE}_{\text{ST}} \tag{55}$$

The switching function is now redefined during the stay time:

$$\hat{S} = |\boldsymbol{\lambda}_v + \boldsymbol{\xi}|/m - \lambda_m/c, \qquad t_1 \le t \le t_2 \tag{56}$$

The thrust unit direction vector is also redefined during the stay time:

$$\boldsymbol{u} = (\boldsymbol{\lambda}_v + \boldsymbol{\xi})/|\boldsymbol{\lambda}_v + \boldsymbol{\xi}| \tag{57}$$

The costate equations (13) and (21) are also affected:

$$\dot{\boldsymbol{\lambda}}_r = -(\boldsymbol{\lambda}_v + \boldsymbol{\xi})^T \left(\frac{\partial \boldsymbol{g}}{\partial \boldsymbol{r}}\right) \tag{58}$$

$$\dot{\lambda}_m = \frac{|\boldsymbol{\lambda}_v + \boldsymbol{\xi}|T}{m^2} \tag{59}$$

Additionally, a set of point constraints, Eqs. (50) and (52), corresponding to the position and velocity state equality constraints must be adjoined to the Bolza function, either at t_1 or at t_2 (Ref. 9). For this example, the point constraint is adjoined at time t_1. The new Bolza function is

$$G = m_f + \boldsymbol{\omega}_0^T \psi_0 + \boldsymbol{\omega}_1^T \psi_1 + \boldsymbol{\omega}_f^T \psi_f + \theta_1\left(t_2 - t_1 - t_{\text{stay}} - s_1^2\right) + \theta_2\left(t_f - t_0 - \text{TOF} + s_2^2\right) \tag{60}$$

Using these new definitions for the Bolza function and the Hamiltonian, the first-order differential conditions for optimality can be determined. There are three new first-order differential conditions

that must be defined as a result of the addition of the Lagrange multipliers adjoined with the state equality constraints' derivatives in the Hamiltonian:

$$H_{\xi} = \mathbf{SE}_{\mathrm{ST}} = [(T/m)\boldsymbol{u} + \boldsymbol{g} - \boldsymbol{a}_T]_{3\times 1} = 0 \tag{61}$$

$$T\boldsymbol{u} = m[\boldsymbol{a}_T - \boldsymbol{g}] \tag{62}$$

This equation must be satisfied across the stay time trajectory and defines the thrust vector during the stay time. For this problem, the term in brackets in Eq. (62) is equal to zero because the acceleration of the target body is equal to the gravitational acceleration the spacecraft experiences at the position of the target. Because the thrust unit direction vector $\boldsymbol{u}$ is a nonzero quantity, the thrust magnitude T must be equal to zero across the entire stay time. However, if the target were not a planet but possibly another vehicle that is itself thrusting, the simplifications to Eq. (62) would not be valid, and the spacecraft could have nonzero thrust.

The other first-order necessary conditions correspond identically with Eqs. (28–39) except for Eq. (37). This condition is now modified as it is a function of the physical position and velocity constraints at t_2, which are no longer included in the Bolza function when using the state equality constraint. Equation (37) is replaced with another condition:

$$\boldsymbol{\lambda}_{2-} = \boldsymbol{\lambda}_{2+} \tag{63}$$

Equation (36) then yields

$$G_{t2} = \theta_1 = H_{2+} - H_{2-} = \hat{S}_{2+}T_{2+} - \hat{S}_{2-}T_{2-} - \left(\boldsymbol{\xi}^T \mathbf{SE}_{\mathrm{ST}}\right)_{t2-} + \left(\boldsymbol{\xi}^T \mathbf{SE}_{\mathrm{ST}}\right)_{t2+} \tag{64}$$

Combining this with the result that thrust is zero at the end of the stay time (i.e., at t_{2-}), the fact that the state equality constraint is equal to zero during the stay time (i.e., at t_{2-}), and the fact that the Lagrange multipliers adjoined to the state equality constraint are zero on the inbound trajectory (i.e., at t_{2+}) yields

$$S_{2+}T_{2+} - \theta_1 = 0 \tag{65}$$

Combining Eqs. (32) and (33) yields

$$S_{1-}T_{1-} - \theta_1 = 0 \tag{66}$$

Therefore, although the first-order conditions were different in form for the state equality constraint formulation, the results of the two formulations are identical as shown in Eqs. (65) and (66), which match the boundary targets found using a mass discontinuity in Eqs. (45) and (47) and the conditions found using the two corner control discontinuities.[4] Therefore, the multipliers needed at time t_2 for the optimal trajectory are the same when solving the problem using the state equality constraint or the two corner control discontinuities. The state equality constraint formulation is a more rigorous definition of the problem and verifies the other results.

Sample Missions

Solutions are generated using a nonlinear boundary-value solver from the Harwell Subroutine Library.[§] It is a hybrid algorithm that uses Newton–Raphson and steepest descent methods combined with a Broyden method to improve the Jacobian matrix to solve the multipoint boundary-value problem.

Optimal Round-Trip CSI Trajectories with Mass Discontinuities

Running various missions with mass discontinuities at the target system produced some interesting results, particularly for CSI Jupiter missions. For most mission profiles, the slack variables, which allow the inequalities in the stay time and the total time of flight, were driven to zero. This indicates that the optimal solution lies along the specified boundary. In particular, for the unbounded VSI engines the two slack variables will always be driven to zero as the extra degree of freedom of the VSI engine is best exploited over the longest duration burn times for the outbound and inbound trajectory legs. However, for CSI engines and VSI engines with bounds on either the thrust or I_{sp} the slack variables are not necessarily always driven to zero. Nonzero slack variables were found for Jupiter CSI missions using an I_{sp} of 5000 s, a power level of 5 MW, a 1460-day maximum round-trip time, and a 365-day minimum stay time. An initial mass of 100 mT was specified in this case, and the final mass value is maximized. The departure dates are in December 2017. Additionally, a negative mass discontinuity was introduced at Jupiter, and a parametric scan of mass drop-offs was analyzed. At first, for small mass drop-offs both slack variables were driven to zero, and the optimal total time of flight was at the limit of 1460 days. However, once the mass drop-off was increased past 7.5 mT, the total TOF slack variable becomes nonzero, and the optimal total time of flight is less than 1460 days. The total time of flight then decreases in a linear fashion as the mass drop-off at Jupiter increases in magnitude as shown in Fig. 2. This result was very interesting and demonstrates the capabilities of the optimal control theory governing the optimization of these round-trip trajectories. These optimal trajectories that lie off the boundaries of the time inequality constraints demonstrate that the solution space is increased when using such constraints. The inequality time constraints are useful and are a more general optimization formulation than the fixed, user-specified values used by Casalino and Colasurdo[1] and Casalino et al.[2]

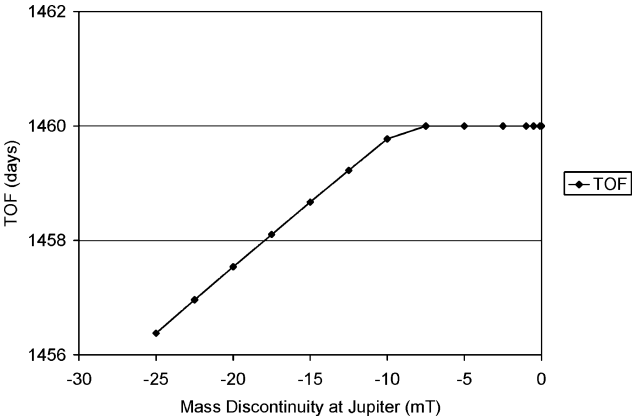

Fig. 2 CSI Jupiter TOF vs mass discontinuity.

Examining the switching function for these trajectories with the nonzero slack variable also yields interesting results. For an optimal solution, the initial and final switching functions are equal from Eq. (49). When along the total time-of-flight boundary, they must also be nonzero as the multiplier θ_2, adjoined to total time of flight inequality constraint, is nonzero when the slack variable is zero as required by Eq. (34). However, when the optimal solution is off the boundary with a nonzero slack variable, the value for θ_2 is driven to zero, and the switching functions at t_0 and t_f must not only equal each other, but must equal zero. This is shown in Fig. 3, which plots an optimal round-trip Jupiter trajectory with a mass drop-off of 17.5 mT. The plot also shows that the inequality constraint boundary associated with the stay time is still active, and therefore the switching functions at t_1 and t_2, while equal, are nonzero.

I_{sp} or Thrust Constraints and Mass Discontinuities on VASIMR Missions

Placing upper and lower bounds on the I_{sp} or thrust values reduces the effectiveness and limits the added degree of freedom the VSI engine has compared with a CSI engine. However, the results for missions run using a VASIMR-like range of I_{sp} of 3000–30,000 s are still much more efficient than a comparable CSI engine. The engines examined use a maximum power level of 5 MW. Optimal VSI trajectories with the I_{sp} constraints were found, which included

[§]Data available online at http://www.cse.clrc.ac.uk/nag/hsl/ [cited 18 July 2003].

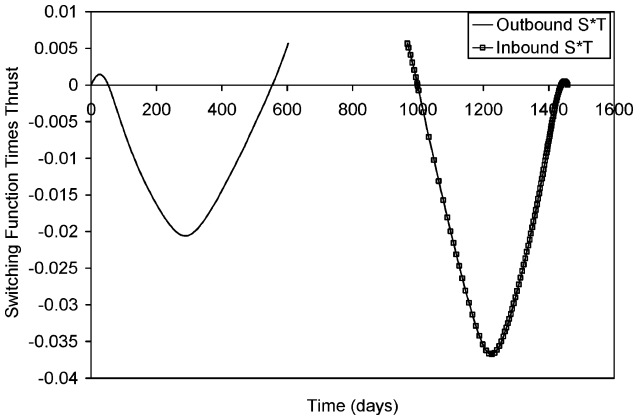

Fig. 3 CSI Jupiter switching function vs time ($\Delta m = -17.5$ mT).

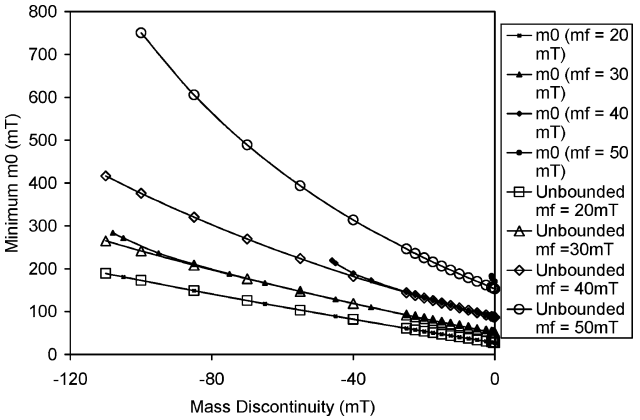

Fig. 4 Unbounded and bounded I_{sp} min m0 for given mf vs mass discontinuity.

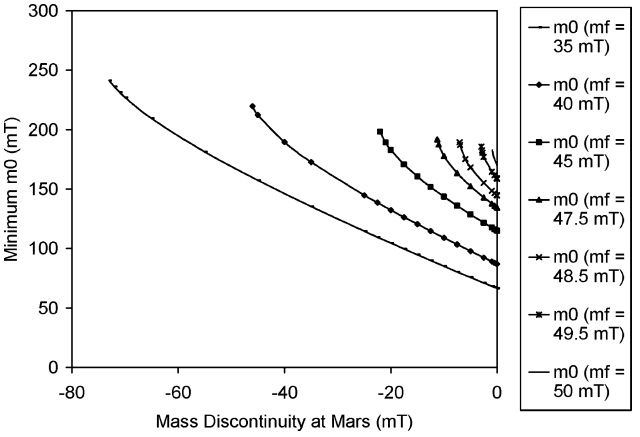

Fig. 5 Mars bounded I_{sp} min m0 for given mf vs mass discontinuities.

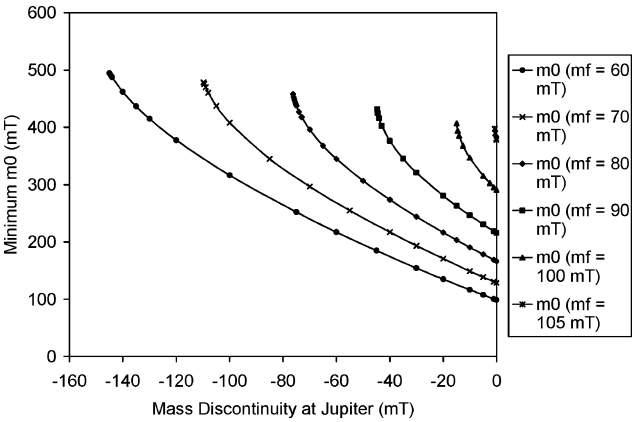

Fig. 6 Jupiter bounded I_{sp} min m0 for given mf vs mass discontinuities.

constant thrust arcs at both the maximum and minimum I_{sp} values and coast periods, along with periods of variable thrust. Additionally, mass discontinuities were introduced to these VSI missions. The minimum initial mass needed was analyzed for a parametric scan of user-specified final mass values and mass discontinuities.

Figure 4 plots one-year round-trip, 60-day stay Mars missions with departure dates in May 2018. Each line of the legend corresponds to a user-specified final mass. The plot shows the minimum initial mass needed for each user-specified final mass as the mass discontinuity is parametrically varied. Only negative mass discontinuities are considered. The figure plots values found for both unbounded and bounded I_{sp} missions. It strikingly shows the effects of the bounds on the I_{sp}. For missions with low final mass values such as 20 or 30 mT, the minimum initial mass for the unbounded I_{sp} and bounded I_{sp} mission are almost identical as the magnitude of the mass drop-off increases from 0 to 110 mT. Some significant separation is seen for the 30 mT final mass case for mass drop-offs larger than 85 mT. However, bounded I_{sp} missions are not controllable for a final mass of 30 mT with mass drop-offs greater than 108 mT. At this point, the bounded I_{sp} engine needs approximately 20 mT more initial mass than the unbounded mission. It was not possible to get missions to converge with mass drop-offs larger than 108 mT with 30 mT user-specified final mass. A much sharper disparity between the unbounded and bounded I_{sp} missions is seen for larger specified final mass values such as 40 and 50 mT. The bounded I_{sp} 40 mT final mass mission becomes uncontrollable for mass drop-offs larger than 73 mT, and the bounded I_{sp} 50 mT final mass mission is uncontrollable for mass drop-offs larger than 0.9 mT. Figure 4 shows that the unbounded I_{sp} missions with final mass values of 40 and 50 mT converge for a much larger range of mass drop-offs (shown here up to 110 mT) than the bounded case. Clearly, the I_{sp} bounds of 3000–30,000 s can greatly reduce the mission capability.

Figure 5 removes the unbounded solutions and shows only the bounded I_{sp} missions shown in Fig. 4. The final data point on the left of each curve corresponds to the final converged trajectory before the engine starts becoming uncontrollable. For larger magnitude mass discontinuities than the leftmost points on each line, it was not possible to get trajectories to converge. A linear curve connecting each of these terminal points represents an upper bound for possible missions using this engine and mission time constraints. This is a controllability ceiling for the engine for this type of mission. Trajectories that fall above this curve are infeasible given this set of mission and engine parameters. To make such missions achievable, some of the mission or engine parameters such as the stay time, time of flight, engine power, and I_{sp} or thrust bounds must be modified. Figure 5, which plots Mars missions, and Fig. 6, which plots Jupiter missions, can be very useful in mission planning. By specifying the final mass upon Earth return and the mass to be dropped off at the target system, the user can determine first if the mission is possible, and, if so, the minimum initial mass needed to achieve such a mission.

Figure 6 plots the same pattern of data for round-trip Jupiter missions, again showing a controllability ceiling for the engine. The total time of flight for these missions is 1460 days, and the minimum stay time at Jupiter is 365 days.

Conclusions

The methodology presented in this paper allows a rigorous optimization of many round-trip trajectories using realistic engine models. The addition of mass discontinuities and specific impulse I_{sp} or thrust bounds for variable-specific-impulse (VSI) engines allows trajectories to be generated that account for these conditions in actual missions. Using these optimization capabilities an engine's controllability ceiling showing its feasible and infeasible regions can be

found, as shown here for VSI round-trip missions with I_{sp} bounds and a mass drop-off at the target. The feasible missions shown are for a 5-MW engine with the I_{sp} bounded between 3000 and 30,000 s. The missions presented target Mars with a one-year round-trip time and 60 days at Mars and target Jupiter with a four-year round-trip time and one year at Jupiter. The inequalities in the stay time and total time of flight are shown to be useful in finding optimal trajectories as shown for constant-specific-impulse Jupiter missions, where the optimal round-trip trajectory is actually more efficient with a shorter total time of flight than the user-specified maximum time.

Additionally, the boundary-value problem posed by analyzing the round-trip trajectory as an optimal control problem with two control discontinuities at the arrival and departure from the target has been verified by reformulating the problem. By approaching the round-trip trajectory as an optimal control problem with a state equality constraint requiring the spacecraft to have zero relative position and velocity with respect to the target system during the stay time, the original boundary-value problem is derived with the same unknown and constraint vectors. This technique also allows for the target to be a body undergoing acceleration forces other than gravity, for example, a thrusting spacecraft. Future work might also consider a minimum heliocentric distance constraint and the escape and capture spiral dynamics.

References

[1]Casalino, L., and Colasurdo, G., "Optimization of Variable-Specific-Impulse Interplanetary Trajectories," *Proceedings of the AIAA/AAS Astrodynamics Conference,* AIAA, Reston, VA, 2002; also AIAA Paper 2002-4897, Aug. 2002.

[2]Casalino, L., Colasurdo, G., and Pastrone, D., "Optimization Procedure for Preliminary Design of Opposition-Class Mars Missions," *Journal of Guidance, Control, and Dynamics*, Vol. 21, No. 1, 1998, pp. 134–140.

[3]Pontryagin, L. S., Boltyanskii, V. G., Gamkrelidze, R. V., and Mishchenko, E. F., *The Mathematical Theory of Optimal Processes*, Wiley-Interscience, New York, 1962, pp. 9–75.

[4]Ranieri, C. L., and Ocampo, C. A., "Optimization of Roundtrip, Time-Constrained, Finite Burn Trajectories via an Indirect Method," *Journal of Guidance, Control, and Dynamics*, Vol. 28, No. 2, 2005, pp. 306–314.

[5]Chang-Diaz, F., "The VASIMR Rocket," *Scientific American*, Vol. 283, No. 5, 2000, pp. 90–97.

[6]Lawden, D. F., *Optimal Trajectories for Space Navigation*, Butterworths, London, 1963, pp. 79–94.

[7]Ocampo, C., "Finite Burn Maneuver Modeling for a GeneralizedTrajectory Design and Optimization System," *Astrodynamics, Space Missions, and Chaos*, Annals of the New York Academy of Sciences, Vol. 1017, May 2004, pp. 210–233.

[8]Hull, D. G., *Optimal Control Theory for Applications*, Springer-Verlag, New York, 2003, pp. 276–316.

[9]Bryson, A., and Ho, Y. C., *Applied Optimal Control: Optimization, Estimation, and Control*, Hemisphere, Washington, DC, 1975, pp. 90–128.